



1 **Frozen debris lobe morphology and movement: an**
2 **overview of eight dynamic features, southern Brooks**
3 **Range, Alaska**

4
5 **Margaret M. Darrow,¹ Nora L. Gyswyt¹, Jocelyn M. Simpson¹, Ronald P.**
6 **Daanen², Trent D. Hubbard²**

7 ¹Department of Mining and Geological Engineering, University of Alaska Fairbanks,
8 Fairbanks, Alaska 99775, USA

9 ²Alaska Division of Geological & Geophysical Surveys, Fairbanks, Alaska 99709, USA

10 *Correspondence to:* Margaret M. Darrow (mmdarrow@alaska.edu)

11

12 **Abstract**

13 Frozen debris lobes (FDLs) are elongated, lobate permafrost features, many of which are
14 present within the Brooks Range of Alaska. We present a comprehensive overview of eight
15 FDLs within the Dalton Highway corridor, including their catchment geology and rock
16 strengths, lobe soil characteristics, surface movement measurements collected between 2012
17 and 2015, and analysis of historic and modern imagery from 1955 to 2014. Field mapping
18 and rock strength data indicate that the metasedimentary and metavolcanic bedrock forming
19 the majority of the lobe catchments has very low to medium strength and is heavily fractured,
20 thus easily contributing to FDL formation. The eight investigated FDLs consist of platy rocks
21 typical of their catchments, organic debris, and an ice-poor soil matrix; massive ice, however,
22 is present within FDLs as infiltration ice, concentrated within cracks open to the surface.
23 Exposure of infiltration ice in retrogressive thaw slumps (RTSs) and associated debris flows
24 lead to increased movement and various stages of destabilization, resulting in morphological
25 differences among the lobes. Analysis of historic imagery indicates that movement of the
26 eight investigated FDLs has been asynchronous over the study period. Since 1955, six of the
27 eight investigated lobes demonstrated an increase in movement rates. The formation of
28 surface features, such as cracks, scarps, and RTSs, suggest that the increased movement rates
29 correlate to general instability, and even at their current distances, FDLs are impacting



1 infrastructure through increased sediment mobilization. FDL-A is the largest of the
2 investigated FDLs. As of August 2015, FDL-A was 39.2m from the toe of the Dalton
3 Highway embankment. Based on its current distance and rate of movement, we predict that
4 FDL-A will reach the current Dalton Highway alignment by 2023.

5

6 **1 Introduction**

7 A warming climate has been identified as unequivocal by the Intergovernmental Panel on
8 Climate Change (IPCC), with greater and faster temperature increase and an overall
9 precipitation increase demonstrated at northern latitudes (Stocker et al., 2013). Analysis of
10 field data collected throughout Arctic and sub-Arctic areas corroborates with IPCC's findings,
11 demonstrating an overall permafrost temperature rise (Christiansen et al., 2010; Romanovsky
12 et al., 2010; Smith et al., 2010). Slopes in permafrost areas are in danger of instability with
13 rising temperatures, as the ice within the soil on the slopes melts and causes loss of soil
14 strength (Geertsema et al., 2006; Gude and Barsch, 2005; Harris et al., 2008a, 2008b;
15 Lewkowicz and Harris, 2005; Swanger and Marchant, 2007). Slope instability presents a risk
16 to adjacent infrastructure especially where roads and utilities pass through mountainous
17 regions. An increase in infrastructure construction may occur in northern regions, including
18 Alaska, as Arctic countries focus on economic development (EOP, 2014; Sevunts, 2013).
19 Thus, recognizing areas of slope instability and quantifying historic and potential movement
20 become progressively important as climate changes and northern regions see increasing
21 development.

22 An example of previous development in the Alaskan Arctic was the construction of the Trans
23 Alaska Pipeline System (TAPS) and supporting infrastructure, including the Dalton Highway,
24 which opened a corridor within the Brooks Range. In the late 1970's and early 1980's, those
25 mapping the geology and geologic hazards along the Dalton Highway corridor noted the
26 presence of elongated, lobate features along slopes adjacent to the highway, thought to be
27 inactive at that time (Hamilton, 1978, 1979, 1981; Kreig and Reger, 1982; Brown and Kreig,
28 1983). These features were "rediscovered" in 2008, partially due to the fact that they were
29 indeed actively moving. When originally mapped, these features were identified as flow
30 slides or rock glaciers; however, ongoing investigations indicate that they are different from
31 rock glaciers in their source, composition, rate and mechanism of movement, and vegetation
32 coverage (Daanen et al., 2012; Simpson et al., in press). Because of these differences, these



1 permafrost features were given the new name *frozen debris lobes* (FDLs) (Daanen et al.,
2 2012). As the resolution of freely-available satellite imagery improves, we continue to
3 identify additional FDLs, with nearly 160 FDLs located thus far within the Brooks Range
4 (Figure S1).

5 Much work has been done to describe and categorize mass wasting features on permafrost-
6 stabilized slopes in mountain regions (French, 2007; Gorbunov and Seversky, 1999; Gruber
7 and Haeberli, 2007; Humlum, 1998a; Kääb et al., 2007; Matsuoka et al., 2005; Wahrhaftig
8 and Cox, 1959). FDLs are the latest features to be defined (Daanen et al., 2012), representing
9 one part in the continuum of permafrost creep features (Haeberli et al., 2006). Since FDLs
10 were referred to previously as rock glaciers, we include a brief summary of these features for
11 comparison. Rock glaciers are described in many cold climate regions (Ballantyne et al.,
12 2009; Barsch, 1977; Berthling et al., 2003; Bollman et al., 2015; Brenning and Azocar, 2010;
13 Calkin et al., 1998; Farbrot et al., 2007; Haeberli et al., 2006; Humlum, 1998a, 1998b; Isaksen
14 et al., 2000; Kääb et al., 1997, Wahrhaftig and Cox, 1959; Wirz et al., 2015), typically
15 forming on talus slopes, at the base of cliffs, or within cirques (Davis, 2001; Embleton and
16 King, 1975). These features often demonstrate surfaces composed of blocky debris, which
17 may be underlain by finer material (Embleton and King, 1975; Ikeda and Matsuoka, 2006;
18 Wahrhaftig and Cox, 1959). In Alaska's Brooks Range, Calkin et al. (1987) hypothesized that
19 rock glaciers formed just after Pleistocene glacial retreat. Ellis and Calkin (1984) suggested
20 that these rock glaciers probably formed from increased rockfall from oversteepened valleys
21 and cirque walls after the late Pleistocene glaciation, resulting in mostly glacier-cored rock
22 glaciers.

23 In terms of lobe geometry, Matsuoka et al. (2005) describe a classification for rock glaciers
24 and solifluction lobes. FDLs most resemble these authors' description for "pebbly" rock
25 glaciers; however, the dimensions of FDLs are typically much greater and their debris does
26 not resemble pebbles. Rock glaciers typically move 1 m yr^{-1} or less, although recent
27 measurements show rates as high as 6.3 m yr^{-1} (Micheletti et al., 2015; Wirz et al., 2015). We
28 show in this paper that FDLs move at rates an order of magnitude greater than those typical of
29 rock glaciers. Another characteristic of FDLs that sets them apart from most rock glaciers is
30 their vegetative cover. Many of the FDLs within the Dalton Highway corridor support mature
31 white spruce forests on their surfaces and all support brushy vegetation; the trees indicate
32 movement of the underlying FDL by their orientations away from vertical. Forested rock
33 glaciers do exist, such as Tien Shan rock glaciers in Central Asia (Sorg et al., 2015) and the



1 Slims River lobate rock glacier in Canada (Blumstengel and Harris, 1988); however, their
2 slower rates of movement and, in the case of the Slims River rock glacier, its icy matrix set
3 these rock glaciers apart from FDLs, as we show below.

4 Field investigations of FDLs began in 2008 with preliminary differential global positioning
5 system (DGPS) measurements, soil pits, and field observations on FDL-A, with some work on
6 nearby FDL-B, -C, and -D (Daanen et al., 2012). Due to its close proximity to the Dalton
7 Highway, we conducted a subsurface investigation of FDL-A jointly with the Alaska
8 Department of Transportation and Public Facilities (ADOT&PF) in September 2012 (Darrow
9 et al., 2012, 2013). Simpson et al. (in press) focused on the geotechnical and GIS analysis of
10 FDL-A, presenting the results of strength testing of frozen soil samples and a slope stability
11 analysis, and the initial results of a GIS protocol by which to examine FDLs. Results from
12 these early investigations indicate that FDLs are mainly composed of a fine-grained soil
13 matrix, but also contain rocks and organic debris. Data from instrumentation installed within
14 FDL-A indicate that this frozen debris lobe moves through a combination of shear in a zone
15 20.6 to 22.8m below ground surface (bgs) and through temperature-dependent internal flow
16 (Darrow et al., 2015; Simpson et al., in press). The average internal temperature of the lobe is
17 -1.1°C below the depth of zero annual amplitude, whereas the temperature of the adjacent
18 permafrost is -2.2°C . This summary represents the bulk of work conducted thus far on FDLs,
19 ranging from setting the stage for FDL analysis through the presentation of preliminary results
20 and interpretation (Daanen et al., 2012), to a more in-depth focus on FDL-A (Darrow et al.,
21 2012, 2013, 2015; Simpson et al., in press).

22 In 2013 we expanded the Area of Interest (AOI) to include eight FDLs (Figure 1). Since
23 expanding the investigation, we have traveled to the field two to three times a year to collect
24 DGPS measurements of the FDL surfaces, as well as samples of soil, rock, water, and ice.
25 Our field investigations and observations led us to the following questions. 1) How does the
26 bedrock source geology contribute to FDL morphology? 2) Are the investigated FDLs
27 consistent in composition and morphology? 3) Has the movement of these FDLs been
28 synchronous? 4) Have their rates of movement changed over time? 5) How can we describe
29 the origin of these features? 6) How are FDLs impacting infrastructure? In an effort to
30 answer these questions, in this paper we present for the first time a comprehensive overview
31 of eight different FDLs within the Dalton Highway corridor. Within this overview, we detail
32 catchment geology, and measured rock strengths and lobe soil characteristics. To illustrate
33 current and historic rates of movement, we present DGPS surface movement measurements



1 collected between 2012 and 2015; and analysis of aerial imagery, satellite imagery, and Light
2 Detection and Ranging (LiDAR) data collected between 1955 and 2014. We also present the
3 results of stable isotope analysis of ice and water samples and radiocarbon dating results of
4 organic soil samples from FDL-A, used to determine its origin and long-term record of
5 movement.

6

7 **2 Methods**

8 **2.1 Fieldwork and sample collection**

9 We selected eight FDLs to assess their geohazard potential based on their size, evidence of
10 movement, and proximity to the Dalton Highway. The planned field study consisted of
11 measuring surface movement rates, and collecting samples for rock strength and soil index
12 property testing. During field visits, we also walked each of the FDLs to evaluate the lobes'
13 surface characteristics, identifying notable features such as scarps, retrogressive thaw slumps
14 (RTSs) and exposed ice, thermokarsts, split trees, etc. The field investigations sometimes
15 yielded unforeseen opportunities to collect samples for special testing, as discussed below.

16 To determine current rates and spatial variability of surface movement, we installed surface
17 marker pins on the eight FDLs. We began by installing the surface marker pins on FDL-A in
18 late October 2012, which we have since measured two to three times a year (typically in
19 March or April, June, and August). In June 2013, we installed surface marker pins on the
20 other seven FDLs under investigation. On each lobe, the surface marker pins were positioned
21 along a longitudinal profile from the catchment to the lobe toe, and along at least one cross-
22 sectional transect. We made repeated measurements of all surface marker pins in August
23 2013, June and August 2014, and May and August 2015. Measurements were made with a
24 DGPS unit, having horizontal and vertical accuracies of ± 5 cm. In addition to establishing
25 the surface marker pin locations, we located and mapped easily visible scarps in the less-
26 vegetated catchment areas with a hand-held GPS. RTSs are present in several FDL
27 catchments and on the lobes. On return visits, we remapped the head scarps of the RTSs to
28 determine rates of regression.

29 We collected rock and soil samples (Figure S2) to determine rock strengths and soil
30 engineering index properties. We sampled rocks from the catchment areas for strength
31 testing, while also updating the pre-existing geologic map of the area (Spangler and Hubbard,



1 in review). Once back in the laboratory, tests were made with a hydraulic point-load testing
2 device to determine the rocks' point load strength indices, which were converted to uniaxial
3 compressive strengths. On each lobe, we dug two 1m deep soil pits, examining the near
4 surface soils and collecting samples for standard engineering index property testing, including
5 moisture content [ASTM D2116], organic content [modified from AASHTO T267], grain size
6 distribution [AASHTO T27/T11, ASTM D422], and plasticity [ASTM D4318] (AASHTO,
7 2009; ASTM, 1990, 1998, 2000). All soil classifications are based on the Unified Soil
8 Classification System (USCS). We also sampled buried organic material from the lower
9 catchment of FDL-A, sending the sampled soil to Beta Analytic, Inc. for radiocarbon dating.
10 This laboratory service calibrated the results using databases associated with the 2013
11 INTCAL program (Reimer et al., 2013), and the resulting two-sigma calendar calibration
12 range is presented here. With this data, we hoped to determine when FDL-A started to move
13 out of the catchment, extending its record of movement beyond the available historic data.

14 The summer of 2014 was the wettest on record for parts of Interior Alaska. As a result,
15 rainfall exposed massive ice in several RTSs on FDL-7, -A, and -D. Seizing the opportunity
16 to determine the origin of the massive ice, in August 2014 we collected samples of exposed
17 ice on FDL-A in the lower RTS near the left flank (see lower arrow in Figure 2a), as well as
18 water samples from the creek that drains FDL-A and a puddle adjacent to the lobe during a
19 major rain event; in March 2015, we collected two samples of snow from the lobe. These
20 samples were submitted for analysis to the Alaska Stable Isotope Facility at the University of
21 Alaska Fairbanks' Water & Environmental Research Center. The purpose of the isotope
22 analysis was to determine the relative age of the ice, and thus identify its probable origin.
23 Stable isotope data were obtained using continuous-flow isotope ratio mass spectrometry
24 (CFIRMS). The $\delta^{2}\text{H}$ and $\delta^{18}\text{O}$ values were measured using pyrolysis-EA-IRMS. This
25 method utilized a ThermoScientific high temperature elemental analyzer (TC/EA) and Conflo
26 IV interface with a DeltaVPlus Mass Spectrometer. Stable isotope ratios were reported in δ
27 notation as parts per thousand (‰) deviation from the international standards, V-SMOW
28 (Standard Mean Ocean Water). Typically, instrument precision is $<3.0\text{‰}$ for hydrogen and
29 $<0.5\text{‰}$ for oxygen.

30 **2.2 Historic image collection and analysis**

31 We acquired aerial and satellite imagery for the AOI from years between 1955 and 2014
32 (Table 1); images for each dataset were compiled into mosaics using the Agisoft Photoscan



1 and ENVI software. The mosaics were ortho-rectified according to the American Society of
2 Photogrammetry and Remote Sensing's (ASPRS) horizontal accuracy standards (ASPRS,
3 2015). In a GIS environment, we used contour lines derived from digital elevation models
4 (DEMs) produced from 2011 LiDAR and 2001 Interferometric Synthetic Aperture Radar
5 (IfSAR) data (1m and 5m resolution, respectively), GPS measurements, and field observations
6 as references for determining catchment and 2011 lobe extents. Next, we determined the
7 extent of each lobe for each year of available imagery (spatial limitations in imagery coverage
8 are summarized in Table 1). Because the FDLs demonstrate downslope movement with only
9 minor lateral spreading, longitudinal profile polylines oriented along the center of each lobe
10 served as the consistent reference from which to measure changes. Historic movement of
11 each FDL was analyzed by measuring the progression of the toe of the lobe between each set
12 of data years. Although not part of the rate analysis, we also include assessment of 2001 and
13 2002 Google Earth images of the AOI in the discussion.

14

15 **3 Results**

16 The results from the various FDLs have been grouped as appropriate in the following
17 discussion. When multiple FDLs are discussed or presented in figures and tables, they are
18 presented from the north to the south (see Figure 1 for FDL spatial distribution within the
19 AOI).

20 **3.1 Catchments and rock data**

21 Frozen debris lobes typically originate from catchments (Figure 2a), many of which may have
22 supported small cirque glaciers during early to mid-Pleistocene glacial advances in the area
23 (Hamilton, 1986). In some cases, FDLs have formed at the base of a slope rather than a
24 catchment, from the accumulation of loose colluvium (e.g., FDL-C), or from landslide
25 deposits (Figure 2b). The catchments of the eight FDLs presented here range from 121,000
26 m² (FDL-B) to 801,000 m² (FDL-A), with an average size of 414,000 m² (Table S1).

27 The catchments of the investigated FDLs range from bowl-like and well-defined (FDL-11, -B,
28 -A, -D, -5), to flatter with more open slopes (FDL-7, -4). The upper portions of the
29 catchments typically consist of exposed rock talus and solifluction lobes supporting shrubby
30 vegetation (Figure 2c). The major sources of debris coming into the catchments are rock fall
31 and solifluction (Daanen et al., 2012; Spangler et al., 2013).



1 The bedrock contributing to the studied catchment areas consists of heavily fractured,
2 metasedimentary and metavolcanic rocks, including phyllite, slate, metasiltstone,
3 metasandstone, greywacke, and conglomerate, with minor amounts of limestone, marble, and
4 igneous intrusions (Figure S2; see Table S2 for rock unit descriptions). The joint spacing is
5 typically less than 30mm. The rocks tested had strengths ranging from 14.0 to 77.3 MPa
6 (Figure S2, Table S1), which covers the range from very low strength to medium strength
7 (Kehew, 2006). It should be noted that testing was conducted on samples that were
8 competent enough to be collected and transported from the field, which suggests that these
9 strength values are an overestimate of the actual rock strengths in the field area. While the
10 bedrock in each catchment consists of different units, the commonality among all catchments
11 is the predominance of heavily fractured, platy, foliated rocks. Additionally, while some
12 samples demonstrated medium strength values, the test results and associated bedrock
13 geology indicate that most of the catchment areas are underlain by very low to low strength
14 rocks. The combination of low strength and high degree of fracturing suggests that much of
15 the bedrock can be treated as dense coarse soil (Milligan et al., 2005), thus easily contributing
16 to the formation of mass movement features such as FDLs.

17 **3.2 Frozen debris lobe composition and morphology**

18 FDLs are elongate lobate features. The areas of the eight FDLs presented here range from
19 83,000 m² (FDL-11) to 286,000 m² (FDL-A), with an average area of 149,000 m². Their
20 length-to-width ratios typically range from 4:1 to 7:1 (Table S3). An exception is FDL-C,
21 with a length-to-width ratio of 2:1. The rounder appearance of this lobe is most likely due to
22 its origin at the base of a slope rather than in a catchment, which limits both its supply of
23 debris and water. Most notable about the surface of FDL-C are the smaller, superimposed
24 surface lobes that form as the mass moves downslope (Figure 2d). These features are present
25 on several other lobes, including FDL-A. Analysis of subsurface data suggests that the
26 surface lobes form as faster internal flow within the active layer becomes sandwiched between
27 the cooling surface and the rising permafrost table in the fall (Darrow et al., 2015). Soil pits
28 excavated into the top 1 m of several of the lobes contained buried organic layers, possibly
29 buried as the surface was overrun by uphill material in a surface lobe.

30 Unlike their morphological cousins the rock glaciers, FDLs are composed of platy rocks
31 typical of their catchments, organic debris such as trees and shrubs, and a soil matrix typically
32 composed of silty sand with varying amounts of gravel, all of which is frozen (Table S3).



1 Where sampled, the upper 1m of tested FDL soils were moist to wet and slightly organic to
2 organic. Similar tests were conducted on the subsurface samples obtained from the 2012
3 drilling on FDL-A. Samples were collected from depths ranging from 2.9 to 24.8m bgs, and
4 tested uniformly as wet (when thawed) silty sand with gravel (Table S3), indicating a
5 consistency in the soil gradation and moisture content with depth that may occur for all FDLs.
6 Boreholes from the 2012 subsurface investigation intercepted no massive ice, and all samples
7 obtained from the drilling were ice-poor (i.e., <1% ice by volume).

8 While the soils are generally ice-poor, massive ice does exist within FDL-A and other FDLs.
9 Over several years, we have measured and observed the changes of two RTSs on the lobe's
10 surface (Figure 2a). For example, we photographed the change in the upper RTS on FDL-A
11 (Figure 3), which retreated up to 20m between 2011 and 2015. This rapid retreat is due
12 mostly to the melting of massive ice, which the significant rainfall of 2014 helped to expose.

13 While there are several different origins of massive ice in periglacial regions (Davis, 2001;
14 Washburn, 1985; Williams and Smith, 1989), we propose that the ice exposed in the FDLs is
15 infiltration ice, which forms as rain and snow melt quickly freeze after entering into cracks in
16 the ground; Tarussov (1992) used the term "infiltration ice" to describe a similar phenomenon
17 produced as summer melt infiltrates glacial ice. The ice we observed in the head scarps of the
18 RTSs was clear consisting of large crystals, and containing bubbles and strands of fungus
19 (Figure 4a inset). Observations of the head scarp in the lower RTS further support the
20 infiltration ice origin. In Figure 4a, the exposed massive ice is indicated in the center of the
21 photograph, with a buried organic layer vertically offset to its right and left, indicating
22 downslope movement. The location of the massive ice corresponds with an open surface
23 crack.

24 Figure 4b is a presentation of the isotope analysis results, with the Global Meteoric Water
25 Line (GMWL) plotted for comparison. The infiltration ice sample plots close to the average
26 of the creek and puddle samples collected during the 2014 summer. The average of the snow
27 samples is somewhat lighter. Isotope values from massive ice bodies taken from the literature
28 also are presented in Figure 4b. These include values from Pleistocene wedge ice near
29 Fairbanks, Alaska (Douglas et al., 2011), lateglacial and Holocene wedge ice near Barrow,
30 Alaska (Meyer et al., 2010), and a suite of wedge ice samples ranging in age from Pleistocene
31 to recent from northern Siberia (Meyer et al., 2002). This collection of data indicates that the
32 oldest ice has the lightest isotopic composition, which becomes heavier with decreasing age.



1 Most notable is that the infiltration ice sample from FDL-A is bracketed by recent and
2 subrecent wedge ice. The heavy isotopic composition of the infiltration ice and its similarity
3 to the creek and puddle samples supports the hypothesis that infiltration ice forms
4 predominantly from rain water entering cracks open at the surface.

5 Most of the investigated lobes support mature spruce forests whose leaning and cracked trees
6 alert the observer to subsurface movement. This is the case for three lobes, in particular, that
7 represent possible stages in FDL destabilization. Since beginning our field observations, we
8 have noticed increasing signs of instability in FDL-5. Its surface appears to be “deflating” as
9 evident by trees leaning towards its center on both the right and left flanks (Figure 2e). This
10 redistribution of its mass has resulted in oversteepening of the toe, measured at $\sim 44^\circ$ in 2015.

11 FDL-7 on the west side of the Dietrich River represents the next stage in destabilization. This
12 lobe also has deflated with trees leaning towards the center line of the lobe; however, at this
13 more advanced stage, the center has surged forward, forming a lower tongue shape (Figure
14 5a). The lower tongue is actively and quickly changing, with large exposures of bare mineral
15 soil and highly damaged spruce trees (Figure 5b). On the flanks where the lower tongue
16 begins, massive ice and ice-rich soil are exposed in RTSs that generate debris flows and
17 provide another source of surface water during the summer months (Figure 5c). Between
18 May and August 2015, significant erosion occurred, merging the head scarps of the RTSs near
19 the right and left flanks of FDL-7 into one RTS that spans the entire width of the lower
20 tongue.

21 The most advanced stage of destabilization is FDL-D. Between 1993 and 2001, a RTS
22 formed in FDL-D’s lower catchment area. By 2010, transverse cracks in the catchment and
23 longitudinal cracks along the levees were visible and persistent throughout the winter,
24 indicating that the lobe was moving significantly throughout the year (see Figure 6a for an
25 example of transverse cracks within a winter aufeis deposit). Following the formation of the
26 RTS, FDL-D rapidly moved 316m downhill between 2002 and 2014. Although the
27 northernmost scarp has not changed significantly since 2011, other active RTSs continue to
28 enlarge. Our mapping of two other RTSs indicated up to 38m of head scarp retreat between
29 2011 and 2015. These head scarps expose massive ice, which melts and contributes to debris
30 flows. The debris flows cover much of the upper lobe area (Figure 6b), provide additional
31 sediment and water to the lobe, and increase the surface temperature of this already unstable
32 permafrost feature.



1 Downhill of the catchment, the surface of FDL-D is a jumbled landscape, full of cracks,
2 scarps, ponds, bare mineral soil, and crisscrossed vegetation that once was a mature spruce
3 forest. Figures 6c and 6d are two examples of the landscape and extreme movement of the
4 surface. In each photograph, a spruce tree is upside down with its roots (Figure 6c) or trunk
5 (Figure 6d) exposed, while the rest of the tree is completely consumed by the lobe.

6 **3.3 Frozen debris lobe movement rates**

7 Figures 7 and 8 are vector maps, illustrating the amount of movement measured on the lobe
8 surfaces between June 2013 and August 2015, as well as RTS head scarp retreat. The lobes
9 were divided into those demonstrating between 6 and 45m of movement (Figure 7), and those
10 demonstrating less than 6m of movement (Figure 8) during the measurement period. The
11 base map data for each of these images is 2011 LiDAR; as some of the FDLs have
12 demonstrated significant movement since then, the 2014 extent of each lobe is included.
13 Movement is generally downhill and parallel to each FDL's longitudinal profile (with FDL-7
14 moving generally eastward, and all other investigated FDLs moving generally westward).
15 Levees that formed along the lobe flanks demonstrate a component of movement away from
16 the center line, indicating some spreading of the lobe along its periphery (see FDL-7, -A, -C,
17 and -4 as examples). Additionally, the levees typically move slower than the rest of the lobe.
18 We observed a notable example of this differential movement in August 2014 on FDL-7 when
19 a recent debris flow along the levee margin was sheared forming echelon cracks within the
20 young deposit (Figure 5c). The average rates of movement for all FDLs for the 2013-2014
21 and 2014-2015 measurement periods are presented in Table S3. These values exclude
22 measurements taken on levees or above the lobes in their catchments. The 2014-2015 rates
23 range from 0.2m yr⁻¹ for FDL-11 to 13.3m yr⁻¹ for FDL-D, with FDL-A falling in between at
24 5.2m yr⁻¹.

25 **3.4 Analysis of historic imagery**

26 Figure 9 is a presentation of the change in extent of the eight investigated FDLs from 1955 to
27 2014. The distance between each pair of toe locations measured along the longitudinal center
28 line for two given data sets was divided by the time interval between data years, resulting in
29 an average movement rate for the time interval. Each rate was assigned to the latter of the two
30 data years (Table S4). These rates were plotted versus time, showing change in movement
31 rate over the total time period from 1955 to 2014 (Figure 10). A drawback to this approach is



1 that it does not capture uneven advancement of the toe due to topographic effects beneath the
2 lobe or differential movement within the lobe; however, the results allowed us to divide the
3 eight FDLs into two general groups, those with increasing rate trends (either steadily or
4 rapidly increasing; Figures 10a and 10b, respectively), and those with decreasing rate trends
5 (Figure 10c). Only two of the eight FDLs have decreasing rate trends.

6 Analysis of the visual progression and rates indicates that movement of these FDLs has been
7 asynchronous over the study period. For example, FDL-11 advanced nearly 10m yr^{-1} in the
8 1970s, faster than any of the other FDLs at that time; however, our surface marker
9 measurements indicate that FDL-11 is currently moving only 0.2m yr^{-1} . In contrast, FDL-D
10 experienced a rapid increase in movement in recent years, moving an average 32.1m yr^{-1}
11 between 2009 and 2011, with FDL-7 and FDL-5 demonstrating the next largest increases in
12 movement rates. FDL-A on the other hand, has demonstrated a steady increase in its
13 movement rate since 1955, fitting a linear trend with a coefficient of correlation (R^2) of 0.88
14 over this period.

15

16 **4 Discussion**

17 The Brooks Range supported massive valley glaciers and ice caps several times during the
18 late Tertiary and Pleistocene (Hamilton 1986). The catchments within the AOI supported
19 cirque glaciers during the Ikillik I advance (110-60 ka), but subsequent advances were not as
20 extensive (Hamilton 1978, 1986). With the retreating ice, debris accumulated in the
21 catchment bottoms. The platy and weak rocks typical of the area weathered to form the silty
22 sand with gravel soil matrix. As the AOI was propitious for the formation of permafrost, the
23 debris froze as it accumulated, providing rheological properties that both countered erosional
24 processes and allowed flow. Accumulation continued until the debris reached a “critical
25 mass” and began to flow out of the catchment areas. The recharge of the debris in the
26 catchment areas is at a much slower rate than the movement rates of the individual lobes; thus,
27 this is the first and only journey these specific features will make downslope. As indicated by
28 Daanen et al. (2012), the end of this mass movement process is an alluvial fan that forms
29 when an FDL completely destabilizes or when it reaches the river in the valley bottom, which
30 removes the toe.

31 When did these FDLs begin to flow from their catchments? We focus on FDL-A for this part
32 of the discussion. FDL-A is farther downslope than any of the other lobes, which suggests



1 that it either began to flow out of its catchment earlier or experienced rapid downslope
2 movement. From field observations and subsequent analysis of LiDAR data, we identified
3 the presence of relatively flat benches along the catchment slopes on either side of FDL-A.
4 We hypothesize that the benches represent the paleosurface of FDL-A before its downslope
5 movement began. Recreating the lobe within the catchment at this level provides a rough
6 volume estimate of 1,450,000 m³ (Figure 11). To test our hypothesis and to determine when
7 the lobe left the catchment, in August 2015 we dug a trench in the active layer on the south
8 bench (see arrow and green dot in Figure 7b). The trench exposed the transition of colluvium
9 (brown organic silt) into typical FDL-A lobe soil (gray silty sand with gravel). Within the
10 lobe soil, we intercepted a buried organic layer, which we sampled for radiocarbon dating.
11 Based on the stratigraphy and its location on the bench, the organic layer was buried (possibly
12 by debris flow deposits) as the lobe surface was actively building. After the lobe reached its
13 critical mass, the center of FDL-A deflated (as currently observed on FDL-7 and FDL-5) as
14 the bulk of the lobe moved downslope, leaving behind the benches and the buried organic
15 material at the lobe's original elevation. The radiocarbon dating returned a calibrated result
16 (95% probability) of Cal AD 1220 to 1285 for the time of burial; thus the major downslope
17 movement of FDL-A began around 730 to 795 years ago.

18 Downslope movement of an FDL causes tension and shearing, which results in the formation
19 of surface cracks. All of the investigated FDLs support numerous transverse and longitudinal
20 cracks, and we suspect that these cracks contain infiltration ice. As a crack opens at the
21 surface due to movement, water entering the crack freezes forming infiltration ice; the crack
22 cannot close again, nor fill with debris. Thus, infiltration ice contributes to FDL movement
23 by providing additional lobe volume. An open, unfilled tension crack represents a break in
24 the subsurface lateral stress distribution (Cornforth, 2005); however, if filled with ice, stresses
25 developed in the upper lobe can be transmitted to the lower reaches. Finally, the ice volume
26 must be considered with increasing temperatures. Increased melting of infiltration ice will
27 lead to reduced soil strength and increased pore water pressure within the lobe (Simpson et al.,
28 in press), which will accelerate FDL movement. Based on the number of surface cracks, an
29 appreciable volume of the FDLs may be ice, certainly more than originally estimated from the
30 2012 subsurface investigation (Darrow et al., 2013).

31 All of the investigated FDLs have scarps or RTSs in their upper reaches (Figures 7 and 8).
32 Analysis of the historic images and Google Earth satellite imagery indicates that the change in
33 lobe morphology and formation of scarps on FDL-7 occurred between 1979 and 1993. The



1 scarps on FDL-A, -C, and -D formed later between 1993 and 2002; the scarps on the other
2 lobes are smaller and difficult to discern in the historic imagery. In the case of FDL-D, the
3 scarp evolved into an active RTS, and subsequently the lobe moved rapidly downslope. We
4 hypothesize that RTS formation is a key step in FDL destabilization. The initial exposure of
5 bare mineral soil increases the surface temperature, which causes infiltration ice to melt
6 (Burn, 2000; Kokelj et al., 2009; Malone et al., 2013). The meltwater forms debris flows that
7 cover a larger area of the lobe, further increasing the surface temperature and repeating the
8 cycle (Gooseff et al., 2009). The debris flows also load the lobe surface with additional
9 sediment, potentially providing the extra driving force needed to initiate downslope
10 movement and the formation of transverse cracks. The meltwater can infiltrate through the
11 now open cracks to the basal shear zone, increasing pore water pressure and further
12 accelerating the lobe's movement. More movement perpetuates this process, resulting in
13 overall destabilization.

14 The underlying topography, in addition to RTS formation and increased surface temperatures,
15 may contribute to the destabilization of FDLs. Examination of the topographic maps
16 generated from the 1955 imagery and the other historic images indicates that the drainages
17 downslope of FDL-11, -7, -D, and -5 have topographic constrictions that at some point
18 impeded downslope movement of these lobes. The topographic constriction is most obvious
19 for FDL-7. Sometime between 1979 and 1993, the lobe met this topographic narrowing,
20 which halted the movement of the toe of the lobe; however, by 1993 a small portion of the
21 lobe continued to flow forward, forming the lower tongue. The subsequent shearing along the
22 flanks exposed infiltration ice, leading to growth of RTSs and acceleration of FDL-7's lower
23 tongue. We suspect that FDL-5 is only now reaching a topographic constriction and may
24 experience a similar destabilization and increase in movement in the near future.

25 The creeks draining the FDLs modify the permafrost downslope of the lobes, which also may
26 contribute to accelerated movement. For example, we observe that the increased sediment
27 load causes the creeks to jump out of their established channels, causing thermokarsting in the
28 adjacent ice-rich soils (Gooseff et al., 2009). Often these creeks disappear within the
29 permafrost, reappearing farther downhill as springs. This channel migration lowers the
30 permafrost table, and increases ground temperature and pore water pressure, facilitating the
31 movement of the lobe as it slides across the modified terrain. It is through their drainages that
32 even the most-distant FDLs are impacting the infrastructure. The increased sediment
33 mobilization from FDL movement and destabilization fills ditches and culverts, resulting in



1 an overtopping hazard to the Dalton Highway and increased maintenance costs. Even FDL-7,
2 which is across the Dietrich River from the Dalton Highway and TAPS (Figure 1), may affect
3 the infrastructure. The alluvial fan that is building in front of the lobe has the potential to shift
4 the Dietrich River channel to the east impinging on the TAPS alignment.

5 As of August 2015, the eight investigated FDLs range from about 1500 m (FDL-4) to less
6 than 40 m (FDL-A) from the Dalton Highway (Table S3). Given the rate trends presented in
7 Figure 10, we can estimate when each FDL will intersect the highway embankment. Based
8 on its 2015 distance of 39.2m, rate of 5.2m yr⁻¹, and correlation coefficient for rate of
9 movement, we predict that FDL-A will intersect the existing Dalton Highway alignment by
10 2023. This estimate, however, is based on data from 1955 to 2014, which may have been a
11 stable time for FDL-A. The recent enlargement of the upper RTS and the formation of large,
12 persistent transverse cracks across FDL-A mirrors the pattern of instability demonstrated by
13 FDL-D. These features may forecast rapid downslope movement for FDL-A.

14

15 **5 Conclusions**

16 We present the results of the first comprehensive study of eight FDLs, which include repeated
17 surface measurements, rock strength testing, soil engineering index property testing, isotope
18 analysis of infiltration ice, radiocarbon dating, and analysis of historic images of the AOI.
19 Analysis of these various data sets provided answers to initial questions:

- 20 1) The bedrock forming the majority of the catchments has very low to medium strength
21 and is heavily fractured. These characteristics indicate that the bedrock responds
22 quickly and easily to physical weathering processes, and thus contributes to the
23 formation of FDLs.
- 24 2) FDLs consist of platy rocks typical of their catchments, along with organic debris, and
25 an ice-poor soil matrix typically composed of silty sand with varying amounts of
26 gravel. Massive ice is present within FDLs as infiltration ice, concentrated within
27 cracks open to the surface. Increased movement and exposure of ice in RTSs leads to
28 various stages of destabilization, resulting in morphologic differences among the
29 lobes.
- 30 3) Movement of the FDLs within the AOI has been asynchronous since 1955, with FDL-
31 11 demonstrating significant movement in the 1970s followed by quiescence, while



1 FDL-7, -D, and -5 currently demonstrate significant movement and/or increasing signs
2 of destabilization. The radiocarbon dating results provide other evidence of
3 asynchronous movement, indicating that FDL-A began to move out of its catchment
4 over 700 years ago, demonstrating either greater or earlier downslope movement than
5 any of the other FDLs.

6 4) Since 1955, six of the eight investigated lobes demonstrated an increase in movement
7 rates. The formation of surface features, such as cracks, scarps, and RTSSs, suggest
8 that the increased movement rates correlate to general instability.

9 5) We offer a formation scenario of the FDLs after deglaciation of the area, as well as
10 observations on contributing factors to lobe movement and destabilization.

11 6) Even at a distance, FDLs are impacting infrastructure through increased sediment
12 mobilization. Based on its current distance and rate of movement, we predict that
13 FDL-A will reach the current Dalton Highway alignment by 2023; however, this
14 estimate does not account for the signs of increasing instability in the upper reaches of
15 FDL-A.

16 While the results of the research presented here have increased our understanding of the
17 composition, morphology, and movement trends of FDLs, this study is not without
18 limitations. 1) Lack of aerial imagery limited the historic image analysis. Many data sets
19 were unusable due to cloud cover, lighting conditions and shadowing, and damage to the film.
20 Analysis of additional imagery could refine the rate trends, and identify the exact timing of
21 rapid movement for FDL-11, -7, and -D. 2) The organic material sampled from FDL-A
22 provided evidence for its initial downslope movement from the catchment. Similar sample
23 collection should be conducted for the other FDLs to increase the understanding of the history
24 of movement. 3) As in previous studies, the observations presented here indicate that FDL
25 movement is closely tied to air temperature. Unfortunately, long-term temperature data does
26 not exist for the immediate area. Future studies could monopolize on the spruce forests in the
27 area by developing a proxy climate record from tree-ring analysis. 4) From our observations,
28 we suspect that infiltration ice comprises a considerable percentage of FDL volume; however,
29 we cannot estimate this volume based on current data. We recommend the use of geophysical
30 methods combined with additional drilling to determine better estimates of ice. 5) Finally,
31 ongoing measurements of surface movement will provide more refined estimates of rates,
32 allowing field identification of destabilization features.



1

2 **Acknowledgements**

3 The authors thank their colleagues L. Wirth and M. Slife for their expertise and support on
4 this project, and Drs. Shur, Kanevskiy, and Stuefer for their valuable input. This work was
5 funded by grants from the U.S. Department of Transportation (OASRTRS-14-H-UAF-Project
6 B), the Alaska Department of Transportation and Public Facilities (T2-12-17), and through
7 generous support from the Alaska Division of Geological & Geophysical Surveys' Capital
8 Improvement Project and the Alyeska Pipeline Service Company.

9

10 **Disclaimer**

11 The views, opinions, findings, and conclusions reflected in this paper are the responsibility of
12 the authors only and do not represent the official policy or position of the USDOT/OST-R, or
13 any state agency or entity.

14

15 **References**

16 Alaska State Geo-Spatial Data Clearinghouse (ASGDC): Geo-spatial Data.
17 <http://www.asgdc.state.ak.us/>, 2014.

18 American Association of State Highway and Transportation Officials (AASHTO): AASHTO
19 Standard Specifications for Transportation Materials and Methods of Sampling and Testing
20 (Part 2A – Tests), 29th Ed. AASHTO, Washington, D.C., 2009.

21 American Society of Photogrammetry and Remote Sensing (ASPRS): New standard for new
22 era: overview of the 2015 ASPRS positional accuracy standards for digital geospatial data.
23 http://www.asprs.org/a/society/committees/standards/PERS_March2015_Highlight.pdf, 2015.

24 ASTM: D2216 Standard Test Methods for Laboratory Determination of Water (Moisture)
25 Content of Soil and Rock by Mass. ASTM International, West Conshohocken, 1990.

26 ASTM: D422 Standard Test Method for Particle-Size Analysis of Soils. ASTM
27 International, West Conshohocken, 1998.

28 ASTM: D4318 Standard Test Method for Liquid Limit, Plastic Limit, and Plasticity Index of
29 Soils. ASTM International, West Conshohocken, 2000.



- 1 Ballantyne, C. K., Schnabel, C., Xu, S.: Exposure dating and reinterpretation of coarse debris
2 accumulation ('rock glaciers') in the Cairngorm Mountains, Scotland. *Journal of Quaternary*
3 *Science*, 24(1), 19-31, 2009.
- 4 Barsch, D.: Nature and importance of mass-wasting by rock glaciers in alpine permafrost
5 environments. *Earth Surface Processes*, 2(2-3), 231-245, 1977.
- 6 Berthling, I., Etzelmüller, B., Eiken, T., Sollid, J. L.: The rock glaciers on Prins Karls
7 Forland: corrections of surface displacement rates. *Permafrost and Periglacial Processes*, 14,
8 291-293, 2003.
- 9 Bollman, E., Girstmair, A., Mitterer, S., Krainer, K., Sailer, R., Stötter, J.: A rock glacier
10 activity index based on rock glacier thickness changes and displacement rates derived from
11 airborne laser scanning. *Permafrost and Periglacial Processes*, 26, 347-359, 2015.
- 12 Blumstengel, W., and Harris, S. A.: Observations on an active lobate rock glacier, Slims
13 River Valley, St. Elias Range, Canada. *Permafrost*, 5th International Conference on
14 *Permafrost*, Trondheim, Norway, 1, 689-694, 1988.
- 15 Brenning, A. and Azocar, G. F.: Statistical analysis of topographic and climatic controls and
16 multispectral signatures of rock glaciers in the Dry Andes, Chile (27°-33° S). *Permafrost and*
17 *Periglacial Processes*, 21(1), 54-66, 2010.
- 18 Brown, J. and Kreig, R. A.: Guidebook to Permafrost and Related Features along the Elliott
19 and Dalton Highways, Fox to Prudhoe Bay, Alaska. *Alaska Division of Geological &*
20 *Geophysical Surveys Guidebook*, Fairbanks, 1983.
- 21 Burn, C. R.: The thermal regime of a retrogressive thaw slump near Mayo, Yukon Territory.
22 *Canadian Journal of Earth Sciences*, 37(7), 967-981, 2000.
- 23 Calkin, P. E., Haworth, L. A., Ellis, C. J.: Rock glacier of Central Brooks Range, Alaska,
24 U.S.A. In Giardino, J. R., Shroder, J. F., Vitek, J. D., eds.: *Rock Glaciers*. Allen and Unwin,
25 Boston, 65-82, 1987.
- 26 Calkin, P. E., Kaufman, D. S., Przybyl, B. J., Whitford, W. B., Peck, B. J.: Glacier regimes,
27 periglacial landforms, and Holocene climate change in the Kigluaik Mountains, Seward
28 Peninsula, Alaska, USA. *Arctic and Alpine Research*, 30(2), 154-165, 1998.
- 29 Cornforth, D. H.: *Landslides in Practice: Investigations, Analysis, and*
30 *Remedial/Preventative Options in Soils*. John Wiley & Sons, Inc., Hoboken, 2005.



- 1 Christiansen, H. H., Etzelmüller, B., Isaksen, K., Juliussen, H., Farbrot, H., Humlum, O.,
- 2 Johansson, M., Ingeman-Nielsen, T., Kristensen, L., Hjort, J., Holmlund, P., Sannel, A. B. K.,
- 3 Sigsgaard, C., Åkerman, H. J., Foged, N., Blikra, L. H., Pernosky, M. A., Ødegård, R. S.: The
- 4 thermal state of permafrost in the Nordic area during the international polar year 2007-2009.
- 5 *Permafrost and Periglacial Processes*, 21, 156-181, 2010.
- 6 Daanen, R. P., Grosse, G., Darrow, M. M., Hamilton, T. D., and Jones, B. M.: Rapid
- 7 movement of frozen debris-lobes: implications for permafrost degradation and slope
- 8 instability in the south-central Brooks Range, Alaska. *Natural Hazards and Earth System*
- 9 *Science*, 12, 1521-1537.
- 10 Darrow, M. M., Daanen, R. P., and Simpson, J. M.: Monitoring and Analysis of Frozen
- 11 Debris Lobes, Phase I: FHWA-RD-AK-12, INE/AUTC 12.25. UAF Institute of Northern
- 12 Engineering, Fairbanks, 2012.
- 13 Darrow, M. M., Daanen, R. P., and Simpson, J. M.: Analysis of a frozen debris lobe: a first
- 14 look inside an impending geohazard. *ISCORD 2013*, 139-148, 2013.
- 15 Darrow, M. M., Simpson, J. M., Daanen, R. P., and Hubbard, T.: Characterizing a frozen
- 16 debris lobe, Dalton Highway, Alaska. *Cold Regions Engineering 2015: Developing and*
- 17 *Maintaining Resilient Infrastructure*, 57-67, 2015.
- 18 Davis, N.: *Permafrost: A Guide to Frozen Ground in Transition*. University of Alaska Press,
- 19 Fairbanks, 2001.
- 20 Dillon, J. T., Harris, A. G., Dutro, Jr., J. T., Solie, D. N., Blum, J. D., Jones, D. L., and
- 21 Howell, D. G.: Preliminary Geologic Map and Section of the Chandalar D-6 and Parts of the
- 22 Chandalar C-6 and Wiseman C-1 and D-1 Quadrangles, Alaska. Alaska Division of
- 23 Geological & Geophysical Surveys Report of Investigation 88-5, 1 sheet, scale 1:63,360,
- 24 1988.
- 25 Douglas, T. A., Fortier, D., Shur, Y. L., Kanevskiy, M. Z., Guo, L., Cai, Y., and Bray, M. T.:
- 26 Biogeochemical and geocryological characteristics of wedge and thermokarst-cave ice in the
- 27 CRREL permafrost tunnel, Alaska. *Permafrost and Periglacial Processes*, 22, 120-128, 2011.
- 28 Ellis, J. M. and Calkin, P. E.: Chronology of Holocene glaciation, central Brooks Range,
- 29 Alaska. *Geological Society of America Bulletin*, 95(8), 897-912, 1984.
- 30 Embleton, C., and King, C. A. M.: *Periglacial Geomorphology*. John Wiley & Sons, New
- 31 York, 203 p., 1975.



- 1 Esri: ArcGIS World Imagery: Electronic data available at:
2 http://goto.arcgisonline.com/maps/world_imagery, 2015.
- 3 Executive Office of the President (EOP): Implementation Plan for the National Strategy for
4 the Arctic Region. Available from [http://www.whitehouse.gov/sites/default/files/docs/](http://www.whitehouse.gov/sites/default/files/docs/implementation_plan_for_the_national_strategy_for_the_arctic_region_-_fi...pdf)
5 [implementation_plan_for_the_national_strategy_for_the_arctic_region – fi...pdf](http://www.whitehouse.gov/sites/default/files/docs/implementation_plan_for_the_national_strategy_for_the_arctic_region_-_fi...pdf), 2014.
- 6 Farbrot, H., Etzelmüller, B., Guomundsson, A., Humlum, O., Kellerer-Pirklbauer, A., Eiken,
7 T., Wangenstein, B.: Rock glaciers and permafrost in Trollaskagi, northern Iceland.
8 *Zeitschrift Fur Geomorphologie*, 51, 1-16, 2007.
- 9 French, H. M.: *The Periglacial Environment*, 3rd Ed. Wiley, Chichester, West Sussex, 458 p.,
10 2007.
- 11 Geertsema, M., Clague, J. J., Schwab, J. W., Evans, S. G.: An overview of recent large
12 catastrophic landslides in northern British Columbia, Canada. *Engineering Geology*, 83(1-3),
13 120-143, 2006.
- 14 Geographic Information Network of Alaska (GINA): Interferometric Synthetic Aperture
15 Radar (IfSAR). 2001.
- 16 Gooseff, M. N., Balsler, A., Bowden, W. B., Jones, J. B.: Effects of hillslope thermokarst in
17 northern Alaska. *EOS*, 90(4), 29-30, 2009.
- 18 Gorbunov, A. P. and Seversky, E. V.: Solifluction in the mountains of central Asia:
19 distribution, morphology, processes. *Permafrost and Periglacial Processes*, 10(1), 81-89,
20 1999.
- 21 Gruber, S. and Haeberli, W.: Permafrost in steep bedrock slopes and its temperature-related
22 destabilization following climate change. *Journal of Geophysical Research – Earth Surface*,
23 112, F02S18, doi:10.1029/2006JF000547, 2007.
- 24 Gude, M., and Barsch, D.: Assessment of geomorphic hazards in connection with permafrost
25 occurrence in the Zugspitze area (Bavarian Alps, Germany). *Geomorphology*, 66(1-4), 85-93,
26 2005.
- 27 Haeberli, W., Hallet, B., Arenson, L., Elconin, R., Humlum, O., Kääb, A., Kaufmann, V.,
28 Ladanyi, B., Matsuoka, N., Springman, S., Mühlh, D. V.: Permafrost creep and rock glacier
29 dynamics. *Permafrost and Periglacial Processes*, 17(3), 189-214, 2006.



- 1 Hamilton, T. D.: Surficial Geologic Map of the Chandalar Quadrangle, Alaska. U.S.
- 2 Geological Survey Miscellaneous Field Studies Map MF-878A, scale 1:250,000, 1978.
- 3 Hamilton, T. D.: Surficial Geologic Map of the Wiseman Quadrangle, Alaska. U.S.
- 4 Geological Survey Miscellaneous Field Studies Map MF-1122, scale 1:250,000, 1979.
- 5 Hamilton, T. D.: Surficial Geologic Map of the Survey Pass Quadrangle, Alaska. U.S.
- 6 Geological Survey Miscellaneous Field Studies Map MF-1320, scale 1:250,000, 1981.
- 7 Hamilton, T. D.: Late Cenozoic Glaciation of the Central Brooks Range. *In* Hamilton, T. D.,
- 8 Reed, K. M., Thorson, R. M., eds.: *Glaciation in Alaska: The Geologic Record*. Alaska
- 9 Geological Society, 9-50, 1986.
- 10 Harris, C., Kern-Luetschg, M., Muron, J., Font, M., Davies, M., Smith, F.: Solifluction
- 11 processes on permafrost and non-permafrost slopes: results of a large-scale laboratory
- 12 simulation. *Permafrost and Periglacial Processes*, 19(4), 359-379, 2008a.
- 13 Harris, C., Smith, J. S., Davies, M. C. R., Rea, B.: An investigation of periglacial slope
- 14 stability in relation to soil properties based on physical modelling in the geotechnical
- 15 centrifuge. *Geomorphology*, 93(3-4), 437-459, 2008b.
- 16 Hubbard, T. D., Koehler, R. D., and Combellick, R. A.: High-resolution lidar data for Alaska
- 17 infrastructure corridors. *Lidar Datasets of Alaska*, Alaska Division of Geological &
- 18 Geophysical Surveys Raw Data File 2011-3, 2011.
- 19 Humlum, O.: The climatic significance of rock glaciers. *Permafrost and Periglacial*
- 20 *Processes*, 9(4), 375-398, 1998a.
- 21 Humlum, O.: Rock glaciers on the Faeroe Islands, the north Atlantic. *Journal of Quaternary*
- 22 *Science*, 13(4), 293-307, 1998b.
- 23 Ikeda, A. and Matsuoka, N.: Pebbly versus bouldery rock glaciers: morphology, structure
- 24 and processes. *Geomorphology*, 73(3-4), 279-296, 2006.
- 25 Isaksen, K., Ødegård, R. S., Eiken, T., Sollid, J. L.: Composition, flow, and development of
- 26 two tongue-shaped rock glaciers in the permafrost of Svalbard. *Permafrost and Periglacial*
- 27 *Processes*, 11(3), 241-248, 2000.
- 28 Kääh, A., Haeberli, W., Gudmundsson, G. H.: Analysing the creep of mountain permafrost
- 29 using high precision aerial photogrammetry: 25 years of monitoring Gruben Rock Glacier,
- 30 Swiss Alps. *Permafrost and Periglacial Processes*, 8(4), 409-426, 1997.



- 1 Kääb, A., Frauenfelder, R., Roer, I.: On the response of rock glacier creep to surface
2 temperature increase. *Global and Planetary Change*, 56(1-2), 172-187, 2007.
- 3 Kehew, A. E.: *Geology for Engineers and Environmental Scientists*, 3rd Ed. Pearson Prentice
4 Hall, New Jersey, 2006.
- 5 Kokelj, S. V., Lantz, T. C., Kanigan, J., Smith, S. L., Coutts, R.: Origin and polycyclic
6 behaviour of tundra thaw slumps, Mackenzie Delta region, Northwest Territories, Canada.
7 *Permafrost and Periglacial Processes*, 20(2), 173-184-2009.
- 8 Kreig, R. A. and Reger, R. D.: *Air-photo Analysis and Summary of Landform Soil Properties*
9 *along the Route of the Trans-Alaska Pipeline System*. Alaska Division of Geological &
10 Geophysical Surveys, Anchorage, 1982.
- 11 Lewkowitz, A. G., and Harris, C.: Morphology and geotechnique of active-layer detachment
12 failures in discontinuous and continuous permafrost, northern Canada. *Geomorphology*,
13 69(1-4), 275-297, 2005.
- 14 Malone, L., Lacelle, D., Kokelj, S., Clark, I. D.: Impacts of hill slope thaw slumps on the
15 geochemistry of permafrost catchments (Stony Creek watershed, NWT, Canada). *Chemical*
16 *Geology*, 356, 38-49, 2013.
- 17 Matsuoka, N., Ikeda, A., Date, T., Morphometric analysis of solifluction lobes and rock
18 glaciers in the Swiss Alps. *Permafrost and Periglacial Processes*, 16(1), 99-113, 2005.
- 19 Meyer, H., Dereviagin, A., Siegert, C., Schirmeister, L., and Hubberten, H.-W.:
20 Paleoclimate reconstruction on Big Lyakhovsky Island, North Siberia – hydrogen and oxygen
21 isotopes in ice wedges. *Permafrost and Periglacial Processes*, 13, 91-105, 2002.
- 22 Meyer, H., Schirmeister, L., Andreev, A., Wagner, D., Hubberten, H.-W., Yoshikawa, K.,
23 Brobrov, A., Wetterich, S., Opel, T., Kandiano, E., and Brown, J.: Lateglacial and Holocene
24 isotopic and environmental history of northern coastal Alaska – results from a buried ice-
25 wedge system at Barrow. *Quaternary Science Reviews*, 29, 3720-3735, 2010.
- 26 Micheletti, N., Lambiel, C., Lane, S. N.: Investigating decadal-scale geomorphic dynamics in
27 an alpine mountain setting. *Journal of Geophysical Research: Earth Surface*, 120, 2155-
28 2175, doi:10.1002/2015JF003656, 2015.



- 1 Milligan, G., Fookes, P. G., and Lee, E. M.: Engineering behaviour of soils and rocks. In
2 Fookes, P. G., Lee, E. M., and Milligan, G., eds., *Geomorphology for Engineers*, CRC Press,
3 Boca Raton, 2005.
- 4 Reimer, P. J., Bard, E., Bayliss, A., Beck, J. W., Blackwell, P. G., Ramsey, C. B., Buck, C. E.,
5 Cheng, H., Edwards, R. L., Friedrich, M., Grootes, P. M., Guiderson, T. P., Hafliðason, H.,
6 Hajdas, I., Hatté, C., Heaton, T. J., Hoffman, D. L., Hogg, A. G., Hughen, K. A., Kaiser, K.
7 F., Kromer, B., Manning, S. W., Niu, M., Reimer, R. W., Richards, D. A., Scott, E. M.,
8 Southon, J. R., Staff, R. A., Turney, C. S. M., van der Plicht, J.: INTCAL13 and MARINE13
9 radiocarbon age calibration curves 0-50,000 years cal BP. *Radiocarbon*, 55(4), 1869-1887,
10 2013.
- 11 Romanovsky, V. E., Smith, S. L., Christiansen, H. H.: Permafrost thermal state in the polar
12 northern hemisphere during the International Polar Year 2007-2009: a synthesis. *Permafrost
13 and Periglacial Processes*, 21(2), 106-116, 2010.
- 14 Sevunts, L.: Canada and Russia stress Arctic economic development. *CBC News*. Available
15 from [http://www.cbc.ca/news/canada/north/canada-and-russia-stress-arctic-economic-
16 development-1.1407697](http://www.cbc.ca/news/canada/north/canada-and-russia-stress-arctic-economic-development-1.1407697)
- 17 Simpson, J. M., Darrow, M. M., Huang, S. L., Daanen, R. P., and Hubbard, T. D.:
18 Investigating movement and characteristics of a frozen debris lobe, South-Central Brooks
19 Range, Alaska. *Environmental and Engineering Geoscience*, (in press).
- 20 Smith, S. L., Romanovsky, V. E., Lewkowicz, A. G., Burn, C. R., Allard, M., Clow, G. D.,
21 Yoshikawa, K., Throop, J.: Thermal state of permafrost in North America: a contribution to
22 the International Polar Year. *Permafrost and Periglacial Processes*, 21(2), 117-135, 2010.
- 23 Sorg, A., Kääh, A., Roesch, A., Bigler, C., Stoffel, M.: Contrasting responses of Central
24 Asian rock glaciers to global warming. *Scientific Reports*, 5:8228, doi:10.1038/srep08228,
25 2015.
- 26 Spangler, E. R., and Hubbard, T. D.: Geologic and geomorphic characterization of frozen
27 debris lobe source basins along the Dalton Highway, southern Brooks Range, Alaska. *Alaska
28 Division of Geological & Geophysical Surveys*, Fairbanks, (in review).
- 29 Spangler, E. R., Hubbard, T. D., Daanen, R. P., Darrow, M. M., Simpson, J. M., and
30 Southerland, L. E.: Geologic and geomorphic characterization of frozen debris lobe



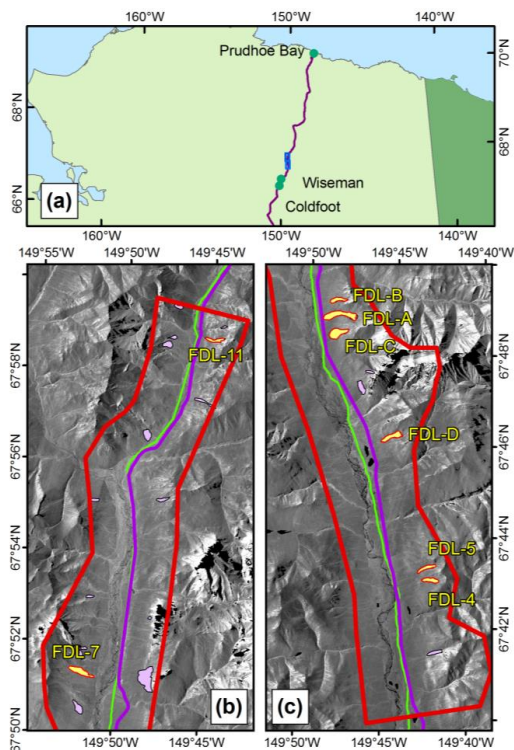
- 1 catchments along the Dalton Highway, southern Brooks Range, Alaska (poster). GSA Annual
2 Meeting, Abstracts with Programs (49-16), 45(7), 152, 2013.
- 3 Stocker, T. F., Qin, D., Plattner, G.-K., Tignor, M. M. B., Allen, S. K., Boschung, J., Nauels,
4 A., Xia, Y., Bex, V., Midgley, P. W., eds., Climate Change 2013: The Physical Science
5 Basis. Working Group I Contribution to the Fifth Assessment Report of the
6 Intergovernmental Panel on Climate Change, Cambridge University Press, Cambridge, 2013.
- 7 Swanger, K. M., and Marchant, D. R.: Sensitivity of ice-cemented Antarctic soils to
8 greenhouse-induced thawing: are terrestrial archives at risk? Earth and Planetary Science
9 Letters, 259(3-4), 347-359, 2007.
- 10 Tarussov, A.: The Arctic from Svalbard to Severnaya Zemlya: climatic reconstructions from
11 ice cores. In Bradley, R. S. and Jones, P. D., Eds.: Climate Since A.D. 1500, Routledge,
12 London, 1992.
- 13 Wahrhaftig, C. and Cox, A.: Rock glaciers in the Alaska Range. Geological Society of
14 America Bulletin, 70, 383-436, 1959.
- 15 Washburn, A. L.: Periglacial problems. In Church, M. and Slaymaker, O., Eds.: Field and
16 Theory: Lectures in Geocryology. University of British Columbia Press, Vancouver, 1985.
- 17 Williams, P. J. and Smith, M. W.: The Frozen Earth: Fundamentals of Geocryology.
18 Cambridge University Press, Cambridge, 1989.
- 19 Wirz, V., Gruber, S., Purves, R. S., Beutel, J., Gärtner-Roer, I., Gubler, S., Vieli, A.: Short-
20 term velocity variations of three rock glaciers and their relationship with meteorological
21 conditions. Earth Surface Dynamics Discussions, 3, 459-514, 2015.
- 22



- 1 Table 1. Summary of available imagery used for historic analysis. USGS is the U.S.
- 2 Geological Survey, AHAP stands for Alaska High-Altitude Photography, and DGGS is the
- 3 Alaska Division of Geological & Geophysical Surveys. If all FDLs are covered by a given
- 4 data set, “NONE” is stated under Limitations.

Year	Source	Resolution (m)	Limitations in FDL coverage
1955	USGS (Aerial)	1.78	NONE
1970	AHAP (Aerial)	2.0	NONE
1978	AHAP (Aerial)	1.5	no FDL-5, -4
1979	AHAP (Aerial)	1.5	only FDL-11, -7, -B
1981	AHAP (Aerial)	1.5	only FDL-D, -5, -4
1993	Quantum Spatial (Aerial)	0.3	NONE
2007	DigitalGlobe Ikonos (Satellite)	1.5	only FDL-7, FDL-B
2009	DigitalGlobe WorldView (Satellite)	0.5	no FDL-11
2011	DGGS (LiDAR)	1.0	NONE
2014	DigitalGlobe WorldView (Satellite)	0.5	NONE

5
 6



1

2 Figure 1. Map of the study area. (a) Location relative to communities along the Dalton
3 Highway (shown in purple); blue rectangular insets show locations of Area of Interest (AOI).
4 The northern and southern portions of the AOI (in red) are shown in (b) and (c), respectively.
5 The eight investigated FDLs are shown in yellow and labeled; other FDLs within the AOI are
6 shown in lavender. The TAPS alignment is indicated in green; within the AOI the
7 infrastructure parallels the Dietrich River. (Base map data from ASGDC (2014) and GINA
8 (2001))

9



18 Figure 2. Typical FDL appearance, lobe, and catchment features. (a) FDL-A, originating
19 from a cirque-like catchment; the Dalton Highway is in the foreground (photograph taken in
20 June 2013). Arrows indicate locations of two retrogressive thaw slumps (RTSs). (b) FDL at
21 the base of a slope outside of the AOI that may have formed from a paleo-landslide deposit.
22 The Trans Alaska Pipeline is in the foreground. (c) FDL-11 catchment, showing typical
23 vegetation and recent scarp; two people stand above the scarp for scale. (d) Riser of smaller
24 surface lobe on FDL-C. (e) Trees near the right flank lean progressively towards the center of
25 FDL-5.

26



1

2

3

4

5

6

7

8

9

10

11

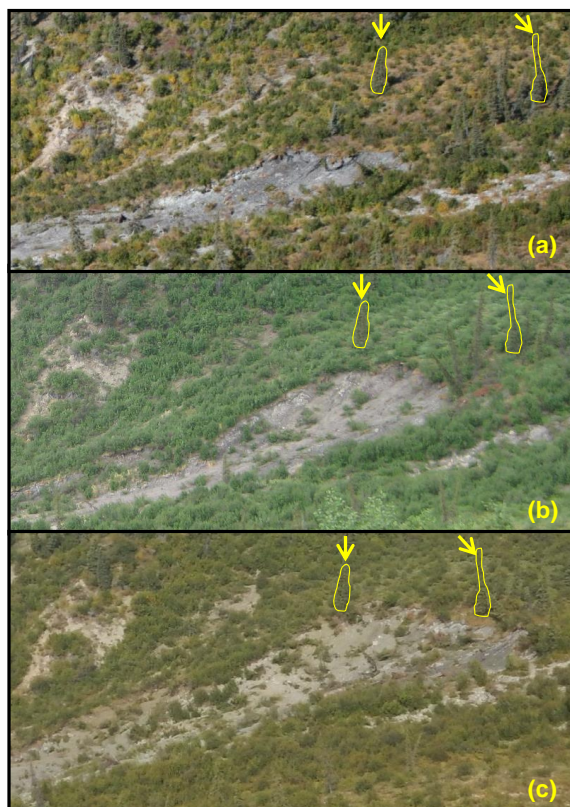
12

13

14

15

16

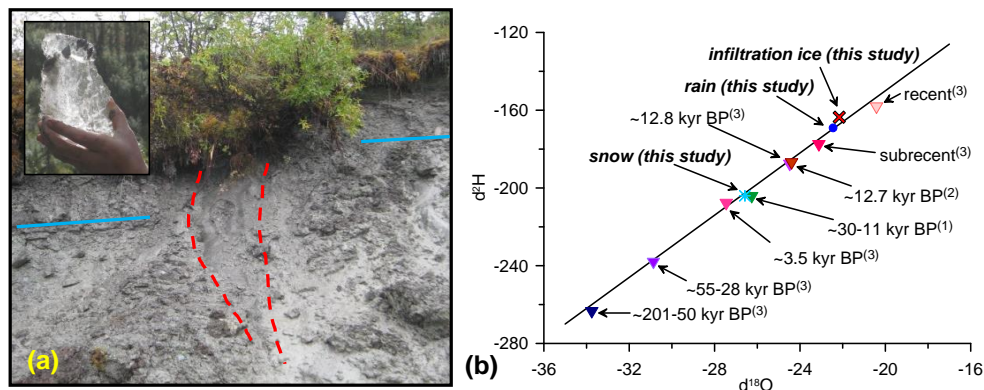


17 Figure 3. Retrogressive thaw slump (RTS) development on FDL-A: (a) August 2008; (b)
18 June 2013; (c) August 2015. Arrows and outlines indicate the same two trees in all three
19 images for comparison.

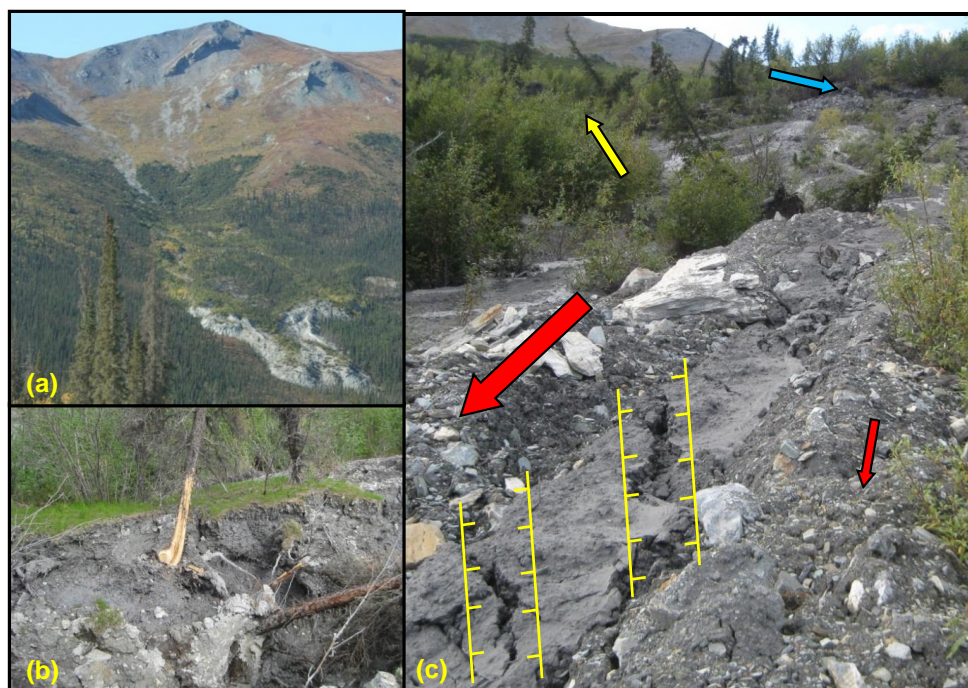
20



1
2
3
4
5
6
7
8
9



10 Figure 4. Infiltration ice in FDL-A. (a) Massive ice (outlined by red dashed lines) exposed in
11 RTS along the left flank in August 2014 (see Figure 2a for location). Offset buried organic
12 layers are indicated by solid blue lines; inset shows example of clear infiltration ice. (b)
13 Isotope analysis results; the GMWL is plotted for comparison. Upside-down triangle symbols
14 represent wedge ice sample values; values taken from the literature are from Douglas et al.
15 (2011)⁽¹⁾, Meyer et al. (2010)⁽²⁾, and Meyer et al. (2002)⁽³⁾.
16

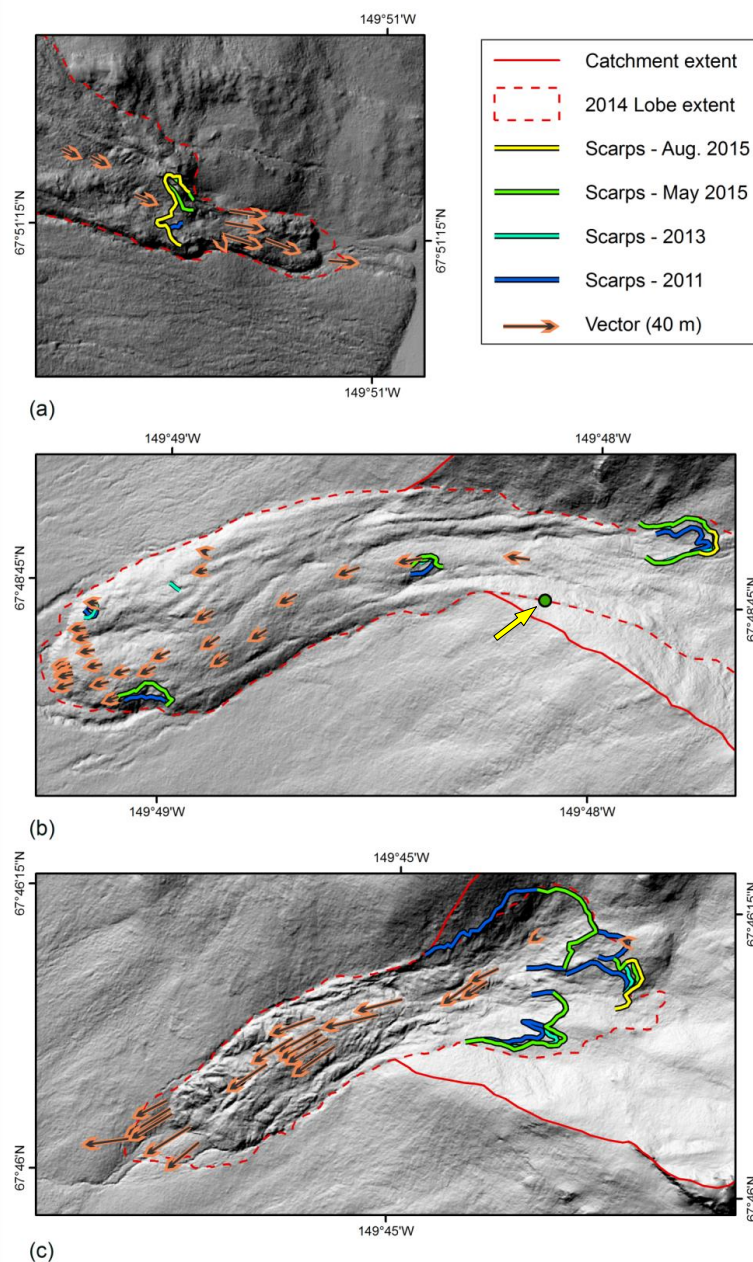


1
2 Figure 5. Features of FDL-7. (a) Deflation of the main lobe body towards the lower tongue,
3 and the major RTSs along the right and left flanks. (b) Vegetation typical of the lower
4 tongue, including a completely split spruce tree demonstrating about 20 cm of previous
5 sedimentation along its trunk. (c) Along the left flank of the lower tongue of FDL-7, differing
6 rates of movement are indicated by the larger red arrow on the lobe and the smaller red arrow
7 on the levee (far right). Echelon cracks are annotated to show extension. The RTS that was
8 the source of the debris flow is indicated by the blue arrow, and an area of leaning trees is
9 indicated by the yellow arrow.

10



16 Figure 6. Destabilization of FDL-D. (a) Evidence of ongoing movement throughout the
17 2014-15 winter and spring, as transverse cracks separate an aufeis deposit on the upper lobe.
18 (b) View down the lobe from the head scarp of one of many RTSs in the catchment, looking
19 over a debris flow originating from the exposed massive ice. (c) Tree completely upside
20 down with root mass sticking out of a crack. (d) Trunk of tree sticking out of debris at toe of
21 FDL-D. Yellow arrows in (c) and (d) point to the tree trunks exiting the lobe surface.
22

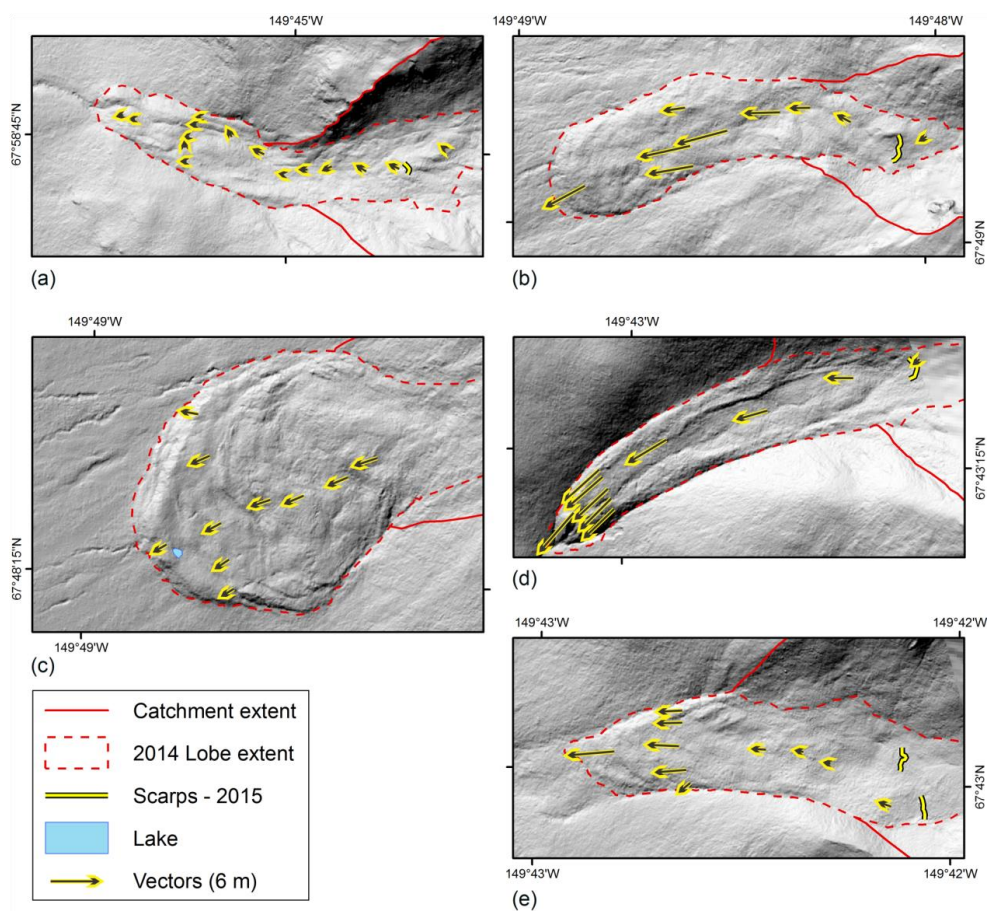


1

2 Figure 7. Vector maps of (a) FDL-7, (b) FDL-A, and (c) FDL-D summarizing movement
3 measured from June 2013 to August 2015, and RTS development. The scale of each image is
4 1:10,000. Vectors are scaled from the 40 m scale included in the legend. The arrow and the



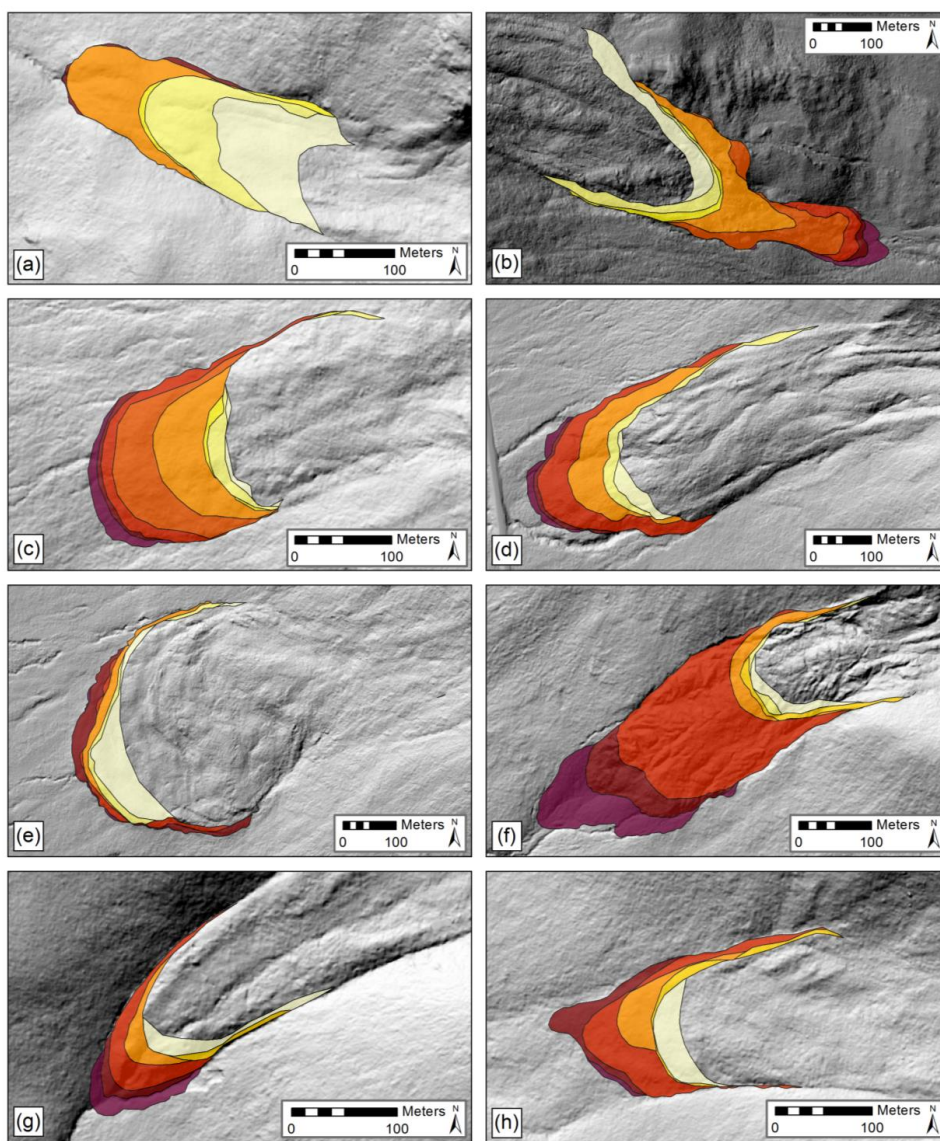
- 1 green dot in (b) indicates the location of sampled organics for radiocarbon dating. (Base maps
- 2 from 2011 LiDAR data (Hubbard et al., 2011))
- 3



1

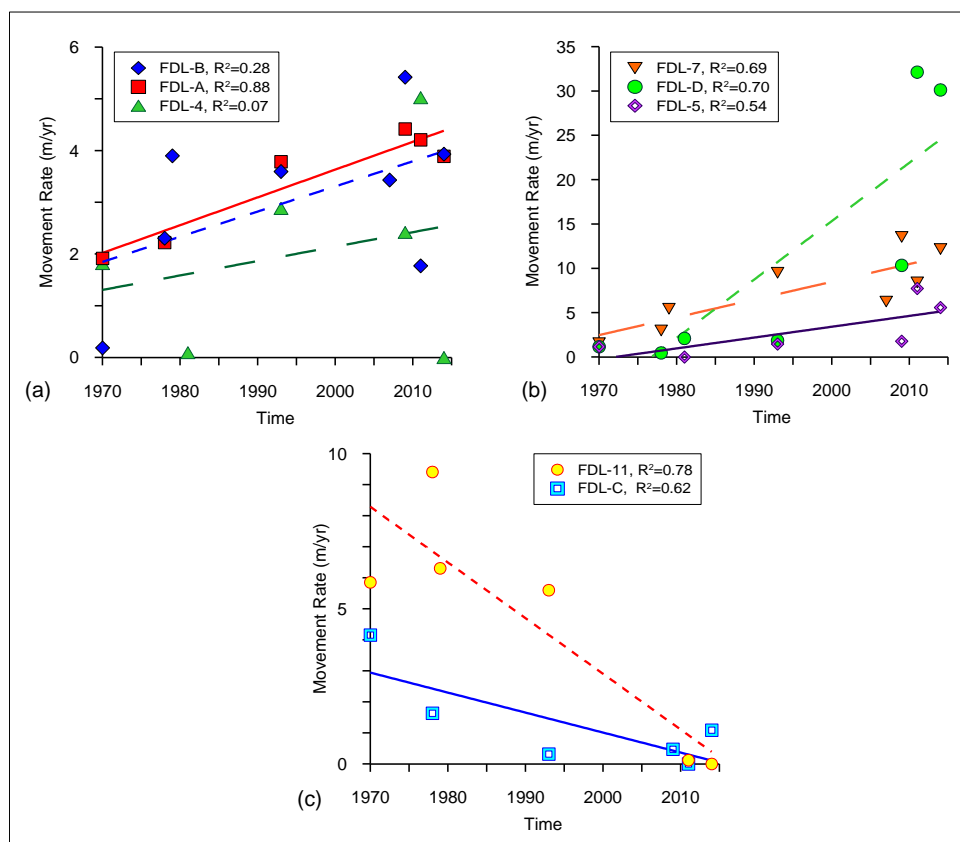
2 Figure 8. Vector maps of (a) FDL-11, (b) FDL-B, (c) FDL-C, (d) FDL-5, and (e) FDL-4
3 summarizing movement measured from June 2013 to August 2015, and scarp locations. The
4 scale of each image is 1:10,000. Vectors are scaled from the 6 m scale included in the legend.
5 (Base map data from Hubbard et al. (2011) and GINA (2001))

6



1
2
3
4
5
6

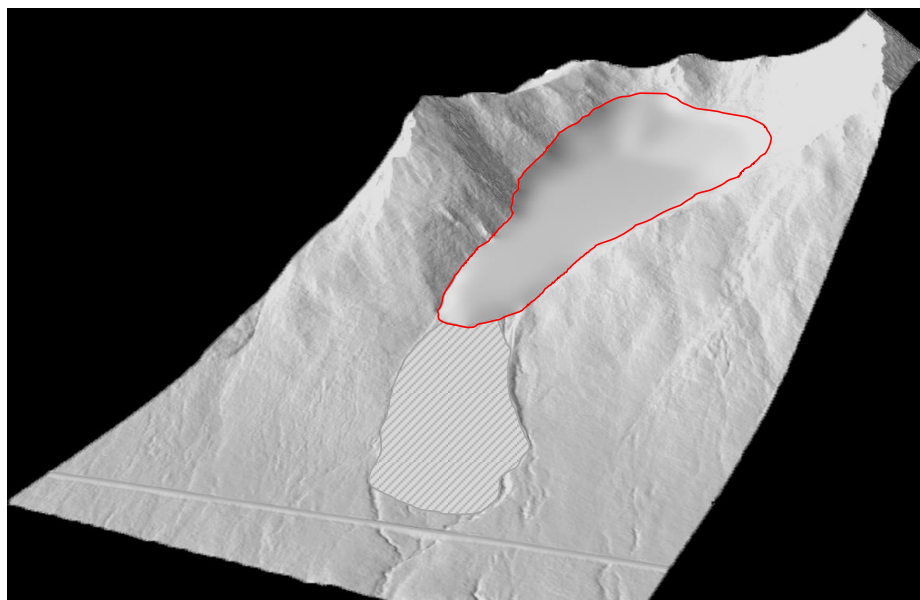
Figure 9. Change in FDL extent from 1955 to 2014: (a) FDL-11, (b) FDL-7, (c) FDL-B, (d) FDL-A, (e) FDL-C, (f) FDL-D, (g) FDL-5, (h) FDL-4. (Base maps from 2011 LiDAR data (Hubbard et al., 2011))



1

2 Figure 10. Historic FDL movement rates from 1955 to 2014 for lobes with (a) steadily
3 increasing rates, (b) rapidly increasing rates, and (c) decreasing rates. The coefficient of
4 correlations (R²) for linear trend lines fit to each lobe data set are presented in the figure
5 legends.

6



1
2 Figure 11. Reconstruction of paleosurface of FDL-A based on bench elevations in its
3 catchment. The reconstructed lobe is outlined in solid red for visibility. The current lobe
4 extent that was removed for the reconstruction is indicated by area with gray diagonal lines.
5 (Base map data from Hubbard et al. (2011))